

# Inverse Problems with Diffusion Models: A MAP Estimation Perspective

Sai bharath chandra Gutha  
KTH, Sweden  
sbcgutha@kth.se

Hossein Azizpour  
KTH, Sweden  
azizpour@kth.se

Ricardo Vinuesa  
KTH, Sweden  
rvinuesa@mech.kth.se

## Abstract

*Inverse problems have many applications in science and engineering. In Computer vision, several image restoration tasks such as inpainting, deblurring, and super-resolution can be formally modeled as inverse problems. Recently, methods have been developed for solving inverse problems that only leverage a pre-trained unconditional diffusion model and do not require additional task-specific training. In such methods, however, the inherent intractability of determining the conditional score function during the reverse diffusion process poses a real challenge, leaving the methods to settle with an approximation instead, which affects their performance in practice. Here, we propose a MAP estimation framework to model the reverse conditional generation process of a continuous time diffusion model as an optimization process of the underlying MAP objective, whose gradient term is tractable. In theory, the proposed framework can be applied to solve general inverse problems using gradient-based optimization methods. However, given the highly non-convex nature of the loss objective, finding a perfect gradient-based optimization algorithm can be quite challenging, nevertheless, our framework offers several potential research directions. We use our proposed formulation and develop empirically effective algorithms for solving noiseless and noisy image inpainting tasks. We validate our proposed algorithms with extensive experiments across diverse mask settings.*

## 1. Introduction

Inverse problems are ubiquitous in science and engineering with a wide range of downstream applications [2, 27]. In Computer vision, several image restoration tasks such as inpainting, deblurring, super-resolution, and more, can be formally modeled as inverse problems. In an inverse problem, characterized by Eq. (1),  $y \in \mathbb{R}^m$  is a (potentially noisy) observation of the original data  $x \in \mathbb{R}^n$ , and  $\eta$  is a random variable denoting i.i.d noise, typically assumed to be Gaussian with a known variance i.e  $\eta \sim \mathcal{N}(0, \sigma_y^2 \mathbb{I})$ , and the task is to infer the original data  $x$  given the observation

$y$ . The function  $\mathcal{A} : \mathbb{R}^n \rightarrow \mathbb{R}^m$  is known as the forward operator, and typically  $n \gg m$ , indicating that the observation  $y \in \mathbb{R}^m$  corresponds to a severely degraded signal, from which one needs to recover the original signal  $x \in \mathbb{R}^n$ , which makes the task highly challenging. For linear inverse problems,  $\mathcal{A}$  denotes a linear mapping and can be substituted with a matrix  $H \in \mathbb{R}^{m \times n}$ .

$$y = \mathcal{A}(x) + \eta \quad (1)$$

Several conventional approaches for solving inverse problems exist [1]. These include approaches based on functional-analytic, probabilistic (bayesian), data-driven methods, and more. Recently, Deep Learning (DL) based methods have been applied to solve inverse problems and have shown great success. In a bayesian framework, solving an inverse problem naturally corresponds to estimating the posterior  $P(x|y)$ . Typical DL-based approaches for solving inverse problems fall into two categories. **1.** Methods that directly learn the posterior  $P(x|y)$  via conditional generative models [13, 18], and **2.** Methods that learn  $P(x)$  via an unconditional generative model and use it to infer  $P(x|y)$  [5, 11, 20, 28]. Methods of the former category require task-specific training, i.e. training with a dataset of pairs  $(x, y)$ , where the degradation  $y$  is computed using  $x$  and a task-specific forward operator  $\mathcal{A}$ . This limits the out-of-the-box applicability of the model to a different task (different forward operator). On the contrary, methods of the latter category train an unconditional generative model to learn  $P(x)$ , and this training is task-independent since it only needs a dataset of original data samples  $x$ . These methods then use the trained model for  $P(x)$  and since  $P(y|x)$  is tractable (i.e from Eq. (1),  $P(y|x) = \mathcal{N}(\mathcal{A}(x), \sigma_y^2 \mathbb{I})$ ), utilizing the bayes rule, they infer the posterior  $P(x|y) \propto P(y|x)P(x)$ .

Several choices for Deep Generative Models (DGMs) exist, each with its advantages and disadvantages. There have been approaches using Generative Adversarial Networks (GAN) [8] and Normalizing Flow (NF) [16] based DGMs for solving inverse problems, with more recent methods focusing on Diffusion models [9, 19, 25], owing

to their state-of-the-art performance in several vision-based generative tasks. In this work, we focus on methods that use a pre-trained unconditional diffusion model as the prior  $P(x)$  and infer the posterior  $P(x|y)$  for solving inverse problems. Sec. 2 provides some background on diffusion models and related works that use unconditional diffusion models for solving inverse problems and their inherent limitations. Later in Sec. 3, we propose our Maximum A Posteriori (MAP) estimation framework for continuous-time diffusion models and discuss the practical implementation. In Sec. 4, we use our proposed framework to develop empirically effective algorithms for image inpainting, and in Sec. 5, we validate our proposed method with extensive experiments on image inpainting across diverse mask settings. Finally, in Secs. 6 and 7, we discuss concurrent works and conclude our findings.

## 2. Background

Given a dataset of samples  $\mathcal{D} = \{x_i\}_{i=1}^N$ , where each  $x_i$  is an i.i.d sample drawn from an unknown data distribution  $P_{data}(x)$ , a generative model learns to approximate  $P_{data}$  from the samples in  $\mathcal{D}$ .

### 2.1. Diffusion Models

Diffusion models [9, 19, 25] are a recent family of generative models. The methodology involves simulating a stochastic process  $\{x(t)\}_{t=0}^T$  described by an SDE (Stochastic Differential Equation) such as Eq. (2), where  $t \in [0, T]$  is a continuous time variable,  $x(0) \sim P_0 = P_{data}$  is the data distribution for which we have a dataset  $\mathcal{D}$  of samples,  $x(T) \sim P_T$  is a tractable prior distribution. The functions  $f(\cdot, t) : \mathbb{R}^n \rightarrow \mathbb{R}^n$  and  $g(\cdot) : \mathbb{R} \rightarrow \mathbb{R}$  are called the drift and diffusion coefficients of  $x(t)$  respectively, and  $dw$  denotes the standard Wiener process. Typically  $f$  and  $g$  are chosen in a way that yields a tractable prior  $P_T$  which contains no information about  $P_0$  (i.e.  $P_{data}$ ).

$$dx = f(x, t)dt + g(t)dw \quad (2)$$

Eq. (2) also describes the "forward process", in which, starting from an initially clean data sample, a small amount of noise is progressively added at each step until it turns into a noisy sample of the prior distribution  $P_T$ . The backward/reverse process which transforms a noisy sample of  $P_T$  into a clean sample of the data distribution is described by the corresponding reverse-SDE in Eq. (3)

$$dx = [f(x, t) - g(t)^2 \nabla_x \log P_t(x)]dt + g(t)d\bar{w} \quad (3)$$

$d\bar{w}$  denotes the standard Wiener process, and  $t$  goes backward from  $T$  to 0 with  $dt$  being an infinitesimal negative time step. The term  $\nabla_x \log P_t(x)$  is called the score function of the marginal distribution  $P_t(x)$ . If we know

this score function for each marginal distribution i.e. for all  $t$ , then one could, in theory, simulate the reverse-SDE in Eq. (3) and generate samples from the data distribution. In general, the score function is not analytically tractable and is hard to estimate, however, one could train a time-indexed neural network model to learn the score function via score matching techniques [24, 26]. The trained score model  $S_\theta(x, t)$  can then be substituted in place of  $\nabla_x \log P_t(x)$  in Eq. (3), and the reverse-SDE can be solved using traditional SDE solvers [25].

$$dx = [f(x, t) - \frac{1}{2}g(t)^2 \nabla_x \log P_t(x)]dt \quad (4)$$

For the stochastic process described by the SDE in Eq. (2), there exists a corresponding ODE (Ordinary Differential Equation) shown in Eq. (4) describing a deterministic process whose trajectories share the same marginal probability densities  $\{P(x_t)\}_{t=0}^T$  as those simulated by the SDE. This is referred to as the probability flow ODE in the literature [25]. So equivalently, one could also use ODE solvers to solve Eq. (4) in reverse time from  $t = T$  until 0 to generate samples from the data distribution.

From hereon, unless mentioned otherwise, we assume the default choice for drift and diffusion coefficients as  $f(x, t) = 0$  and  $g(t) = \sqrt{\frac{d\sigma^2(t)}{dt}}$ , where  $\sigma(t)$  is a monotonically increasing noise schedule from  $t = 0$  to  $T$ , with  $\sigma(T)$  being very high. This choice of  $f$  and  $g$  results in a closed form perturbation kernel  $P(x(t)|x(0)) = \mathcal{N}(x(0), \sigma^2(t) - \sigma^2(0))$  and  $P(x(T)) \approx \mathcal{N}(0, \sigma^2(T))$ . There can be multiple design choices for the noise schedule  $\sigma(t)$ , resulting in various formulations of diffusion models [10].

### 2.2. Solving Inverse problems with Diffusion models

As described in Sec. 1, solving an inverse problem entails estimation of (or sampling from) the posterior  $P(x|y)$ , where  $y$  is the noisy degradation of  $x$  (Eq. (1)). In the context of solving inverse problems using diffusion models, sampling from the posterior  $P(x|y)$  involves conditioning the reverse diffusion process on  $y$  which translates to solving the modified reverse-SDE in Eq. (5).

$$dx = [f(x, t) - g(t)^2 \nabla_x \log P_t(x|y)]dt + g(t)d\bar{w} \quad (5)$$

Similar to methods of the first category (Sec. 1), which directly learn the posterior  $P(x|y)$  as part of their training, it is possible to train a conditional diffusion model that learns the conditional score function directly. More specifically, one could learn  $S_\theta(x, y, t)$  using conditional score matching objectives in place of the usual unconditional score function  $S_\theta(x, t)$  in Sec. 2.1. In this paper, we focus on methods of the second category, which only leverage an unconditional

diffusion model for  $P(x)$ , to infer  $P(x|y)$ . We modify the notations to denote  $P_t(x)$  with  $P(x_t)$  and  $x(t)$  with  $x_t$  for convenience.

$$\nabla_{x_t} \log P(x_t|y) = \nabla_{x_t} \log P(x_t) + \nabla_{x_t} \log P(y|x_t) \quad (6)$$

$$P(y|x_t) = \int_{x_0} P(y|x_0)P(x_0|x_t)dx_0 \quad (7)$$

Solving Eq. (5) involves estimating the conditional score function  $\nabla_{x_t} \log P(x_t|y)$ . The pre-trained unconditional diffusion model can be used to estimate  $\nabla_{x_t} \log P(x_t)$ , however, the term  $\nabla_{x_t} \log P(y|x_t)$  becomes intractable, making it hard to estimate the conditional score (Eqs. (6) and (7)). At its core, the intractability of  $\nabla_{x_t} \log P(y|x_t)$  arises from the fact that  $P(x_0|x_t)$  is intractable [20].

### 2.3. Related works

PGDM [20] approximates  $P(x_0|x_t)$  with a Gaussian distribution having mean  $\hat{x}_t$  and variance  $r_t^2$ , where  $\hat{x}_t = \mathbb{E}(x_0|x_t) = x_t + \sigma^2(t)\nabla_{x_t} \log P(x_t)$  (using Tweedie's formula). The standard deviation  $r_t$  is a hyperparameter, chosen proportionally to  $\sigma(t)$ . DPS [5] approximates  $P(y|x_t)$  with the point estimate  $P(y|x_0 = \hat{x}_t)$  and has an almost similar formulation as PGDM, though the motivation is slightly different. [3] also uses Gaussian approximation but further replace  $r_t$  with the covariance matrix  $Cov[x_0|x_t] = \sigma^2(t)\frac{\partial \hat{x}_t}{\partial x_t}$ . Computing this matrix is expensive in practice, so they resort to diagonal and row-sum approximations of the matrix instead. [15] proposes to find an optimal covariance matrix using learned covariances from the diffusion model. All those methods, however, still rely on making simplified approximations for  $P(x_0|x_t)$ . This limits their performance in practice, given the complicated and multimodal nature of the true data distribution. Other lines of work [6, 7, 11, 29] try to circumvent this term by projecting the intermediate  $x_t$  onto the measurement subspace using heuristic approximations. Some other works [4, 6, 28, 31] pose the problem as a MAP optimization with data and prior terms. Note that our proposed method is quite similar to the concurrent works [4, 28] from a practical perspective. We discuss the similarities and differences later in Sec. 6.

## 3. Our Methodology

### 3.1. Background: Consistency Models

Consider the probability flow ODE described in Eq. (4). The solution trajectories of this ODE are smooth, and maps the samples on the data manifold to pure noise. In [22], a consistency model is defined as the function that map any point on the PF ODE trajectory to its corresponding origin (initial point on the data manifold). There exist efficient methodologies [21] to train these consistency models

in practice. Please refer to [22] for a detailed description of consistency models.

### 3.2. Proposed MAP estimation framework

$$x_0^* = \arg \max_{x_0} \log P(x_0|y) \quad (8)$$

Eq. (8) refers to the usual MAP formulation for solving an inverse problem. Finding an optimal  $x_0^*$  using gradient ascent involves the update step in Eq. (9).

$$x_0^{k+1} = x_0^k + \lambda * \nabla_{x_0} \log P(x_0|y) \quad (9)$$

The update step requires computing the gradient term  $\nabla_{x_0} \log P(x_0|y) = \nabla_{x_0} \log P(y|x_0) + \nabla_{x_0} \log P(x_0)$ . The former term is tractable since  $P(y|x_0)$  is Gaussian, and the latter is the score function evaluated at  $x_0$  and can be replaced with  $S_\theta(x_0, 0)$ .

In practice,  $S_\theta(x_0, 0)$  is only accurate when  $x_0$  lies closer to the data manifold and is typically inaccurate for  $x_0$  in low-likelihood regions outside the data manifold (refer to [23]). This makes the score estimate inaccurate at the start (when  $x_0$  is initialized randomly) and also during the gradient ascent since the intermediate  $x_0^k$  are not constrained to lie on the data manifold. This issue is avoided when inverse problems are typically solved through the reverse diffusion process (Sec. 2.2) which drifts the noisy sample towards the data manifold using  $S_\theta(x_t, t)$  while simultaneously ensuring measurement consistency. But there the bottleneck is to estimate  $\nabla_{x_t} \log P(y|x_t)$  which is intractable, as discussed earlier.

Here, we present our proposed MAP formulation. Let  $z \sim P(x_T) = \mathcal{N}(0, \sigma^2(T)\mathbb{I})$ , denote a purely noisy sample, and  $\mathcal{M}$  denote the data Manifold. The PF ODE trajectory maps  $z$  to a sample  $x_0 \in \mathcal{M}$ , given by  $x_0 = f_\theta(z, T)$ , where  $f_\theta$  is the consistency model. It is also evident that,  $\forall x_0 \in \mathcal{M}, \exists z \sim P(x_T)$  such that  $x_0 = f_\theta(z, T)$ . Hence, the usual MAP formulation in Eq. (8) is equivalent to the proposed MAP formulation in Eqs. (10) and (11).

$$z^* = \arg \max_z \log P(x_0 = f_\theta(z, T)|y) \quad (10)$$

$$x_0^* = f_\theta(z^*, T) \quad (11)$$

With our proposed formulation, we update  $z$  with gradient ascent steps as in Eq. (12) for finding  $z^*$ . The update step now requires computing the gradient term  $\nabla_z \log P(f_\theta(z, T)|y)$ , which can be reformulated as a

vector-jacobian product (vjp) as shown in Eq. (13).

The vector in the vjp from Eq. (13), is the gradient term  $\nabla_{x_0} \log P(x_0|y)$  evaluated at  $x_0 = f_\theta(z, T)$  which lies on the data manifold (by definition of consistency model), and can be accurately evaluated unlike the previous case.

$$z^{k+1} = z^k + \lambda * \nabla_z \log P(f_\theta(z, T)|y) \quad (12)$$

$$\nabla_z \log P(f_\theta(z, T)|y) = \left( \frac{\partial f_\theta(z, T)}{\partial z} \right)^\top \nabla_{x_0} \log P(x_0|y) \Big|_{x_0=f_\theta(z, T)} \quad (13)$$

Here we provide the high-level overview of a practical implementation using our MAP formulation. In practice, even a consistency model  $f_\theta$  can benefit from multi-step sampling [22]. Therefore we propose a multi-step gradient ascent scheme called **MAP-Gradient-Ascent (MAP-GA)** as described in Algorithm 1. Note that  $\tau$  refers to a time-step schedule with  $T = \tau_n > \tau_{n-1} > \dots > \tau_1 > \tau_0 = 0$  and  $\sigma$  refers to the monotonically increasing noise schedule for  $t \in [0, T]$ , with  $\sigma_0 = 0$ , and  $\sigma_T = \infty$  (high value in practice),  $y$  is the measurement,  $f_\theta$  and  $S_\theta$  are the consistency model and the score model respectively.  $num\_iter$  denotes the number of gradient ascent iterations per time step, and  $\lambda$  denotes the learning rate. Algorithm 1 can be applied to solve any inverse problem effectively, given that we know the optimal hyper-parameters, such as the time-step schedule  $\tau$ , the learning rate  $\lambda$ , learning rate schedule,  $num\_steps$ , etc. However, finding those in practice can be quite challenging.

---

**Algorithm 1:** MAP-GA (MAP-Gradient-Ascent)

---

```

input :  $\tau = (\tau_n, \dots, \tau_1, \tau_0)$ ,  $f_\theta$ ,  $S_\theta$ ,  $y$ ,  $num\_iter$ ,  $\lambda$ ,  $\sigma$ 
 $z \sim \mathcal{N}(0, \sigma_{\tau_n}^2 \mathbb{I})$ 
for  $i$  in  $(n, n-1, \dots, 1)$  do
     $t = \tau_i$ 
    for  $j$  in  $(1, 2, \dots, num\_iter)$  do
         $| z = z + \lambda * \nabla_z \log P(f_\theta(z, t)|y)$ 
    end
     $\hat{x}_0 = f_\theta(z, t)$ 
     $z = \mathcal{N}(\hat{x}_0, \sigma_{\tau_{i-1}}^2 \mathbb{I})$ 
end
output:  $z$ 

```

---

### 3.3. Practical Implementation

In practice, to avoid numerical issues, instead of solving for  $x_0^*$ , we solve for  $x_\epsilon^* = \arg \max_{x_\epsilon} \log P(x_\epsilon|y)$ , for a small  $\epsilon$  such that  $\sigma_\epsilon \approx 0$ . So we solve the MAP formulation in Eqs. (14) and (15). Since,  $P(x_\epsilon|x_0) = \mathcal{N}(x_0, \sigma_\epsilon^2 \mathbb{I})$ , for very small values of  $\sigma_\epsilon$ , the distinction between  $x_0$  and  $x_\epsilon$

remain insignificant for all practical purposes. The consistency models in [22] are also learned to map the points on PF ODE trajectory to the corresponding  $x_\epsilon$  instead of  $x_0$ .

$$z^* = \arg \max_z \log P(x_\epsilon = f_\theta(z, T)|y) \quad (14)$$

$$x_0^* \approx x_\epsilon^* = f_\theta(z^*, T) \quad (15)$$

Here, we describe in detail the computation of the gradient term  $\nabla_z \log P(f_\theta(z, t)|y)$  in practice. From Eqs. (16) and (17), this requires the estimation of the gradient of log-likelihood i.e  $\nabla_{x_\epsilon} \log P(y|x_\epsilon)$  and the gradient of log-prior i.e  $\nabla_{x_\epsilon} \log P(x_\epsilon)$ . The terms  $P(y|x_\epsilon)$  and  $P(x_\epsilon)$  are also referred to as the **likelihood** and the **prior** respectively.

$$\nabla_z \log P(f_\theta(z, t)|y) = \left( \frac{\partial f_\theta(z, t)}{\partial z} \right)^\top \nabla_{x_\epsilon} \log P(x_\epsilon|y) \Big|_{x_\epsilon=f_\theta(z, t)} \quad (16)$$

$$\nabla_{x_\epsilon} \log P(x_\epsilon|y) \Big|_{x_\epsilon=f_\theta(z, t)} = \left\{ \nabla_{x_\epsilon} \log P(y|x_\epsilon) + \nabla_{x_\epsilon} \log P(x_\epsilon) \right\} \Big|_{x_\epsilon=f_\theta(z, t)} \quad (17)$$

#### Computing the gradient of log-likelihood

$P(y|x_0) = \mathcal{N}(\mathcal{A}(x_0), \sigma_y^2 \mathbb{I})$ , and  $P(x_\epsilon|x_0) = \mathcal{N}(x_0, \sigma_\epsilon^2 \mathbb{I})$ , given by Eq. (1) and the diffusion perturbation kernel respectively. Since  $\sigma_\epsilon \approx 0$ ,  $P(x_0|x_\epsilon)$  can be approximated with  $P(x_\epsilon|x_0)$ , and for a linear forward operator i.e  $\mathcal{A} = H \in \mathbb{R}^{m \times n}$ , we can derive  $P(y|x_\epsilon) = \mathcal{N}(Hx_\epsilon, \sigma_y^2 \mathbb{I} + \sigma_\epsilon^2 HH^\top)$ . For non-linear  $\mathcal{A}$ , by linearizing it around  $x_\epsilon$ , similar approximations can be derived. As  $\sigma_\epsilon \rightarrow 0$ , these approximations tend to hold well. Given the tractable form of the likelihood term above, computing the gradient of the log-likelihood is apparent.

#### Computing the gradient of log-prior

The gradient of the log prior i.e  $\nabla_{x_\epsilon} \log P(x_\epsilon)$  is essentially the score function evaluated at  $x_\epsilon$ . Given a score function  $S_\theta(x, t)$ , learned by the unconditional diffusion model,  $\nabla_{x_\epsilon} \log P(x_\epsilon) = S_\theta(x_\epsilon, \epsilon)$ . Learning the score function is equivalent to learning a denoiser, and vice-versa [10]. Hereon, we denote the unconditional diffusion model as learning the denoiser  $D_\theta(x, t)$ , from which the score function can be computed as  $\nabla_{x_\epsilon} \log P(x_\epsilon) = \frac{D_\theta(x_\epsilon, t) - x_\epsilon}{\sigma_t^2}$ .

### 4. Image Inpainting with MAP-GA

In Computer vision, image inpainting [14, 30] is a typical image restoration task. Given a masked image (and the corresponding binary mask), the goal here is to recover (reconstruct) the missing pixels of the masked image. Image inpainting can be modeled as a linear inverse problem. Let  $x \in \mathbb{R}^n$  denote the original image,  $y \in \mathbb{R}^m$  denote

a masked image with only visible pixels ( $m \leq n$ ) and  $H \in \mathbb{R}^{m \times n}$  denotes a corresponding forward operator for a given mask. The inpainting problem is characterized by  $y = Hx + \eta$ , where  $\eta \sim \mathcal{N}(0, \sigma_y^2 \mathbb{I})$ . Note that a given mask defines  $H$  and for inpainting,  $H$  has a defined structure, where the rows of  $H$  are one-hot and are orthogonal. This also implies  $HH^\top = \mathbb{I}_{m \times m}$ .

---

**Algorithm 2:** MAP-GA (Algorithm 1 expanded for Inpainting)

---

```

input : time schedule:  $\tau = [\tau_n, \tau_{n-1}, \dots, \tau_1, \tau_0]$ ,
noise schedule:  $\sigma(\cdot)$ , Denoiser:  $D_\theta$ ,
consistency model:  $C_\theta$ ,
measurement:  $y$ , learning rate:  $\lambda$ ,
num gradient ascent iter: num_iter,
boolean: use_prior (default True),
Inpainting matrix:  $H$ ,
Measurement noise:  $\sigma_y$ 
(Note:  $HH^\top = \mathbb{I}_{m \times m}$ ,  $\tau_0 = \epsilon$ ,  $\tau_n = T$ ,
 $z \sim \mathcal{N}(0, \sigma_{\tau_n}^2 \mathbb{I})$ 
for  $i$  in  $(n, n-1, \dots, 1)$  do
     $t = \tau_i$ 
    for  $j$  in  $(1, 2, \dots, num\_iter)$  do
         $\hat{x}_\epsilon = C_\theta(z, t)$ 
         $grad_{likelihood} = \frac{H^\top(y - H\hat{x}_\epsilon)}{\sigma_y^2 + \sigma_\epsilon^2}$ 
        if use_prior then
             $grad_{prior} = \frac{D_\theta(\hat{x}_\epsilon, \epsilon) - \hat{x}_\epsilon}{\sigma_\epsilon^2}$ 
        end
        else
             $grad_{prior} = 0$ 
        end
         $grad_{posterior} = grad_{likelihood} + grad_{prior}$ 
         $grad = \left(\frac{\partial C_\theta(z, t)}{\partial z}\right)^\top grad_{posterior}$ 
         $z = z + \lambda * grad$ 
    end
     $\hat{x}_\epsilon = C_\theta(z, t)$ 
     $z = \mathcal{N}(\hat{x}_\epsilon, \sigma_{\tau_{i-1}}^2 - \sigma_{\tau_0}^2 \mathbb{I})$ 
end
output:  $z$ 

```

---

In this work, to show the effectiveness of our proposed MAP framework in practice, we consider the task of image inpainting with diverse mask settings. We expand Algorithm 1 for the task of image inpainting, and include all the specific details in Algorithm 2. The core quantity in the algorithm that needs to be evaluated is  $\nabla_z \log P(f_\theta(z, t) | y)$ , which involves the estimation of gradients of the log-likelihood and the log-prior terms (Eqs. (16) and (17)). In the algorithm, we make a choice (indicated by the `use_prior` keyword) of retaining or

dropping the gradient of the log-prior. Dropping the prior term implies a choice of uniform prior, and the algorithm now optimizes for the maximum likelihood estimate instead of the MAP estimate, by considering any sample (which is consistent with our measurement) on the data manifold to be equally good. This is also the setting considered in the concurrent works [4, 28].

Note that the algorithm makes use of both the consistency model ( $C_\theta$ ) and the denoiser ( $D_\theta$ ), but this makes the method more demanding compared to other methods that only use the denoiser. For that, we make an argument as follows. We use the pre-trained denoiser and the consistency model from [10] and [22] respectively, with noise schedule  $\sigma(t) = t$  and  $t \in [\epsilon, T]$ , where  $\epsilon = 0.002, T = 80$ . Consider the PF ODE for the above setting, as follows.

$$\begin{aligned}
dx &= -\sigma(t)\dot{\sigma}(t)\nabla_{x_t} \log P(x_t)dt \\
&= -\sigma(t)\dot{\sigma}(t)\frac{D_\theta(x, t) - x}{\sigma^2(t)}dt \\
&= -\dot{\sigma}(t)\frac{D_\theta(x, t) - x}{\sigma(t)}dt \\
&= -\frac{D_\theta(x, t) - x}{t}dt
\end{aligned}$$

This PF ODE determines the trajectory and solving the trajectory origin  $x_0$  involves solving the ODE above. Note that this  $x_0$  is what the consistency model  $C_\theta$  is trained to predict. As a rough approximation, solving the ODE with a backward Euler discretization step from  $t$  to 0, which essentially assumes the trajectory curves are linear, i.e. the jacobian  $\frac{dx}{dt}$  is constant for the interval  $[0, t]$ , and this gives  $C_\theta(x_t, t) = x_0 \approx D_\theta(x_t, t)$ , with the approximation getting more accurate as the trajectory curve gets more linear. In an empirical setting, [10] also observes trajectories become more linear when  $\sigma(t) \rightarrow 0$ . While more analysis on this is still due, it motivates us to look at the denoiser as a proxy of the consistency model, which gradually becomes more and more accurate as  $\sigma(t) \rightarrow 0$ . Hence, we also consider settings that replace the consistency model with the denoiser in our algorithm.

When using Algorithm 2 for noisy image inpainting ( $\sigma_y > 0$ ) in practice, we observe that it requires careful tuning of the learning rate and other hyperparameters. To avoid such additional and sensitive hyperparameters, we present Algorithm 3 for noisy inpainting, based on our empirical observations in Tab. 2. The algorithm requires no additional hyperparameters and works well in practice. The idea behind Algorithm 3, is to find a good approximate solution using MAP-GA at diffusion time  $t = \tau$  where  $\sigma_\tau = \sigma_y$ , and then use it as an initialization for PGDM [20] for  $\sigma_t < \sigma_y$ .

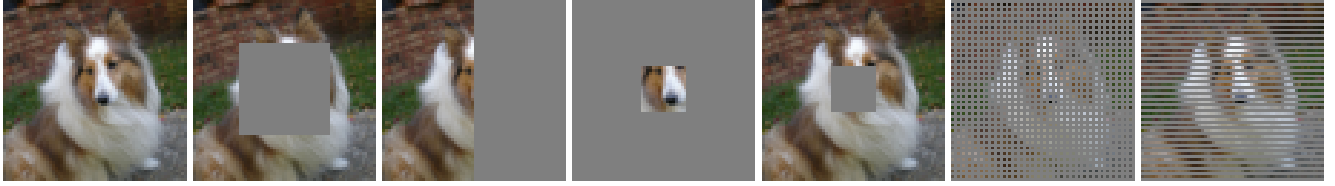


Figure 1. From left to right: original image, and mask settings: box50, half, expand, box25, sr2x, altnlines

---

**Algorithm 3:** MAP-GA-PGDM for Inpainting

---

**input** : noise schedule:  $\sigma(\cdot)$ , Denoiser:  $D_\theta$ , consistency model:  $C_\theta$ , measurement:  $y$ , learning rate:  $\lambda$ , num gradient ascent iter: num\_iter, Inpainting matrix:  $H$ ,  
 Measurement noise:  $\sigma_y$   
 $\tau_{map-ga} = [\tau_n^{map}, \tau_{n-1}^{map}, \dots, \tau_1^{map}, \tau_0^{map}]$ ,  
 $\tau_{pgdm} = [\tau_m^{pgdm}, \tau_{m-1}^{pgdm}, \dots, \tau_1^{pgdm}, \tau_0^{pgdm}]$ ,  
 (Note:  $HH^\top = \mathbb{I}_{m \times m}$ )  
 (Note:  $\sigma_{\tau_0^{map}} = \sigma_y$  and  $\tau_n^{map} = T$ )  
 (Note:  $\sigma_{\tau_m^{pgdm}} = \sigma_y$  and  $\tau_0^{pgdm} = \epsilon$ ),

=====MAP-GA=====

$z \sim \mathcal{N}(0, \sigma_{\tau_n^{map}}^2 \mathbb{I})$   
**for**  $i$  in  $(n, n-1, \dots, 1)$  **do**  
 $t = \tau_i^{map}$   
**for**  $j$  in  $(1, 2, \dots, num\_iter)$  **do**  
 $\hat{x}_\epsilon = C_\theta(z, t)$   
 $grad_{likelihood} = \frac{H^\top (y - H\hat{x}_\epsilon)}{\sigma_y^2 + \sigma_\epsilon^2}$   
 $grad_{posterior} = grad_{likelihood}$   
 $grad = \left( \frac{\partial C_\theta(z, t)}{\partial z} \right)^\top grad_{posterior}$   
 $z = z + \lambda * grad$   
**end**  
 $\hat{x}_\epsilon = C_\theta(z, t)$   
 $z = \mathcal{N}(\hat{x}_\epsilon, \sigma_{\tau_{i-1}^{map}}^2 - \sigma_{\tau_0^{map}}^2 \mathbb{I})$   
**end**

=====PGDM=====

$x_{\tau_m^{pgdm}} = z$   
**for**  $i$  in  $(m, m-1, \dots, 1)$  **do**  
 $t = \tau_i^{pgdm}$   
 $\hat{x}_t = D_\theta(z, t)$   
 $\mu_t = \hat{x}_t + \sigma_t^2 * \nabla_{x_t} \log P(y|x_t) * pgdm\ update*$   
 $x_{\tau_{i-1}^{pgdm}} = \mathcal{N}(\mu_t, \sigma_{\tau_{i-1}^{pgdm}}^2 - \sigma_{\tau_0^{pgdm}}^2 \mathbb{I})$   
**end**  
**output:**  $x_{\tau_0^{pgdm}}$

---

More specifically, we use MAP-GA until  $\sigma_t = \sigma_y$ , to estimate  $x_{\sigma_y}$  and later use this as initialization to PGDM for

$\sigma_t < \sigma_y$ . (Note that we could use  $t$  and  $\sigma_t$  interchangeably in our notations since our noise schedule is  $\sigma(t) = t$ ). We do not use the prior term for the MAP-GA part in Algorithm 3, as we find it more effective.

## 5. Experiments

In all our experiments, we use the pre-trained class-conditional denoiser from [10] and the consistency model from [22] with their default settings. Inspired by [12], we evaluate the inpainting performance across six different mask settings that denote varying levels of degradation. Examples of our mask settings can be seen in Fig. 1. The mask settings *box50* and *box25* indicate a square crop at the center of the image, with the crop width equal to 50% and 25% of the image width respectively. In *half*, we mask out the right half of the image, the mask *expand* is the complement of *box25*. *sr2x* denotes a 2x super-resolution mask, and *altnlines* masks out alternate rows of pixels. We evaluate the inpainted images using FID and LPIPS metrics.

In Tab. 1, we evaluate the performance of MAP-GA (Algorithm 2) for noiseless image inpainting (i.e.  $\sigma_y = 0$ ) on Imagenet [17] validation set with 64x64 resolution having 1k images. In the experiments, the setting MAP-GA denotes the default Algorithm 2, MAP-GA(NP) denotes MAP-GA with no prior, MAP-GA(D) denotes MAP-GA with denoiser replacing the consistency model, and MAP-GA(D,NP) denotes MAP-GA with no prior and the denoiser replacing the consistency model. The results from Tab. 1 show MAP-GA and variants outperforming PGDM by a significant margin. Note that MAP-GA uses gradient ascent (first-order gradient-based optimization algorithm) to optimize the underlying MAP objective which is typically highly non-convex and is not guaranteed to find the global optima. However, with an initialization, closer to the global optima, MAP-GA could converge.

To corroborate this, we design the following toy experiment. We consider the same noiseless inpainting task from earlier, but, in Algorithm 2, we set  $\tau_n = \hat{\tau} \ll T$ , instead of the default setting  $\tau_n = T$  and we also initialize  $z \sim \mathcal{N}(x_0, \sigma_\tau^2 \mathbb{I})$ , where  $x_0$  is the corresponding ground truth image for the measurement  $y$ . From Tab. 2, we observe significant improvements in the performance. (We

Method	box50		half		expand		box25		sr2x		altlines	
	FID $\downarrow$	LPIPS $\downarrow$										
MAP-GA(D,NP)	<b>32.312</b>	<b>0.096</b>	<b>37.986</b>	<b>0.157</b>	93.068	0.419	<b>11.019</b>	<b>0.019</b>	<b>30.072</b>	<b>0.034</b>	<b>18.282</b>	<b>0.015</b>
MAP-GA(D)	35.761	0.100	43.315	0.164	106.32	0.430	11.169	0.019	33.188	0.036	19.103	0.016
MAP-GA(NP)	34.944	0.113	39.243	0.162	<b>69.004</b>	<b>0.388</b>	12.818	0.027	30.303	0.035	20.321	0.018
MAP-GA	36.733	0.113	41.151	0.164	87.952	0.400	12.836	0.027	33.752	0.036	20.895	0.018
PGDM [20]	49.370	0.151	54.261	0.245	127.95	0.479	14.255	0.021	38.433	0.046	20.446	0.019

Table 1. Noiseless inpainting on ImageNet64 1k validation set using MAP-GA and variants. The setting MAP-GA denotes the default Algorithm 2, MAP-GA(NP) denotes MAP-GA with no prior, MAP-GA(D) denotes MAP-GA with denoiser replacing the consistency model, and MAP-GA(D,NP) denotes MAP-GA with no prior and the denoiser replacing the consistency model.

Method	box50		half		expand		box25		sr2x		altlines	
	FID $\downarrow$	LPIPS $\downarrow$										
MAP-GA(D,NP)	26.661	0.043	30.621	0.064	73.510	0.155	<b>9.165</b>	0.010	29.878	0.027	<b>16.971</b>	<b>0.012</b>
MAP-GA(D)	34.689	0.052	41.098	0.083	90.768	0.175	10.891	0.011	34.334	0.031	18.718	0.013
MAP-GA(NP)	<b>25.205</b>	<b>0.043</b>	<b>27.208</b>	<b>0.047</b>	<b>42.671</b>	<b>0.075</b>	10.936	0.017	<b>27.496</b>	<b>0.023</b>	18.732	0.013
MAP-GA	29.508	0.045	33.653	0.050	73.318	0.106	11.257	0.016	34.364	0.026	20.041	0.013
PGDM [20]	31.952	0.056	36.639	0.082	71.352	0.138	10.886	<b>0.009</b>	33.199	0.041	19.551	0.018

Table 2. Noiseless inpainting on ImageNet64 1k validation set. Using the ground truth image ( $x_0$ ) for the measurement  $y$ , we create a sample at  $t = 0.5$  via ( $x_{0.5} = x_0 + 0.5 * \eta$ , where,  $\eta \sim \mathcal{N}(0, \mathbb{I})$ ) and initialize Algorithm 2 with  $z = x_{0.5}$ , and  $\tau_n = 0.5$

use  $\hat{\tau} = 0.5$ , note that  $\sigma_{0.5} = 0.5$ , as we use the noise schedule  $\sigma(t) = t$ ). This shows that MAP-GA is only limited by the choice of optimizer and reinforces the need for better optimization algorithms. While it is important to consider better design choices (for the schedules and hyperparameters), adaptive-gradient-based optimizers (such as momentum, adam), or higher-order methods, we leave this for future work as it requires a thorough analysis.

In Tab. 3, we report the results on noisy inpainting using Algorithm 3 on Imagenet 1k validation set with 64x64 resolution.  $\sigma_y$  indicates the measurement noise and the setting MAP-GA-PGDM denote the default Algorithm 3, MAP-GA-PGDM(D) denote MAP-GA-PGDM with denoiser replacing the consistency model. In Algorithm 3, and all its variants, we fix  $m = 20$  time steps for PGDM. Even with a high level of measurement noise, MAP-GA-PGDM shows promising improvements over PGDM.

In all our experiments, each of our methods has been given a budget of 1000 steps, and we run ablations for (num\_time\_steps, num\_iter) from the set  $\{(20,50),(50,20),(100,10),(200,5),(250,4),(500,2),(1000,1)\}$ . We follow a time-step schedule similar to [10], with their default settings. The best results for all our methods

resulted from the ablation (20,50) denoting 20 time-steps with 50 gradient ascent iterations. For PGDM [20], each setting from our results table is run with different choices of num\_steps from  $\{20,50,100,200,250,500,1000\}$ , and most of the runs have their peak performance at 500 steps. The performance reported in the tables is the best result for each method over the ablations for (num\_time\_steps, num\_iter). The choice of learning rate in all our experiments was  $\sigma_y^2 + \sigma_\epsilon^2$ .

## 6. Discussion

The algorithms presented in this paper are similar to the concurrent works ZSIR [4], and DMPlug [28] from a practical perspective. However, our proposed MAP formulation has a strong theoretical motivation and connects the probability flow ODE and the consistency model with the MAP optimization for solving inverse problems. While we compare only against PGDM [20], it is the most competitive baseline and can also be seen from the experiments in DMPlug [28]. In this work, we analyze our method extensively, on image inpainting with various degradation masks. However, the experiments from DMPlug [28] further complement and validate our work. We show that the gradient of the log-prior is tractable, making the gradient of log-posterior tractable. However, [4, 28] considers an arbi-

Method	$\sigma_y$	box50		half		expand		box25		sr2x		altlines	
		FID $\downarrow$	LPIPS $\downarrow$										
MAP-GA-PGDM(D)	0.05	<b>56.173</b>	<b>0.125</b>	62.026	0.193	108.16	0.438	<b>38.725</b>	<b>0.039</b>	57.41	0.080	46.046	0.046
MAP-GA-PGDM	0.05	58.283	0.147	<b>61.588</b>	<b>0.184</b>	<b>91.508</b>	<b>0.406</b>	44.667	0.085	<b>57.308</b>	<b>0.073</b>	<b>45.265</b>	<b>0.042</b>
PGDM [20]	0.05	77.824	0.175	80.248	0.257	135.99	0.495	53.136	0.049	86.289	0.126	66.203	0.066
MAP-GA-PGDM(D)	0.1	<b>72.543</b>	<b>0.166</b>	79.535	0.230	114.51	0.464	<b>57.556</b>	<b>0.076</b>	76.733	0.145	65.154	0.096
MAP-GA-PGDM	0.1	74.130	0.191	<b>78.322</b>	<b>0.225</b>	<b>103.85</b>	<b>0.440</b>	65.720	0.161	<b>76.248</b>	<b>0.134</b>	<b>63.134</b>	<b>0.089</b>
PGDM [20]	0.1	96.485	0.216	99.170	0.286	145.40	0.519	78.620	0.100	109.47	0.231	90.925	0.138
MAP-GA-PGDM(D)	0.2	91.112	<b>0.243</b>	99.432	0.297	119.45	0.496	<b>79.329</b>	<b>0.154</b>	110.48	0.260	87.727	0.188
MAP-GA-PGDM	0.2	<b>91.087</b>	0.252	<b>97.531</b>	<b>0.296</b>	<b>116.78</b>	<b>0.491</b>	80.647	0.177	<b>103.66</b>	<b>0.248</b>	<b>86.174</b>	<b>0.186</b>
PGDM [20]	0.2	116.81	0.292	117.03	0.344	159.17	0.562	103.43	0.193	132.89	0.366	114.54	0.255

Table 3. Noisy inpainting on ImageNet64 1k validation set.  $\sigma_y$  denotes the measurement noise. The setting MAP-GA-PGDM denotes the default Algorithm 3, MAP-GA-PGDM(D) denote MAP-GA-PGDM with denoiser replacing the consistency model.

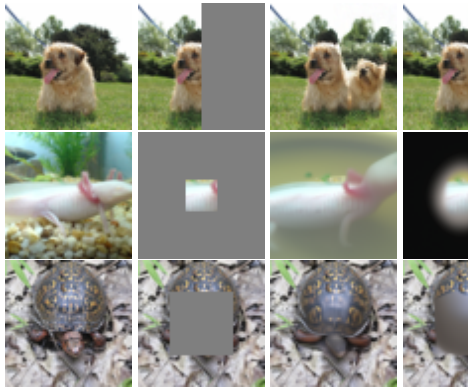


Figure 2. Noiseless inpainting example. From left to right: original image, masked image, MAP-GA(Algorithm 2), PGDM( $\sigma_y = 0$ ). From top to bottom: *half mask*, *expand mask*, *box50 mask*

trary choice of uniform prior and ignores the prior term altogether. We show that MAP-GA is only limited by the choice of the optimizer in practice and our proposed framework has several directions for future research, such as improving optimization with hessian-based methods, more analysis on local optima, theory connecting the denoiser with the consistency model among others. Also, our method and algorithms are valid for general SDE-based Diffusion models and for more general inverse problems than the inpainting task we considered.

## 7. Conclusion

In this paper, we proposed a novel MAP formulation for solving inverse problems using pre-trained unconditional diffusion models. Note that conditional generation is a core requirement in solving inverse problems. We connect the probability flow ODE and the consistency model with the

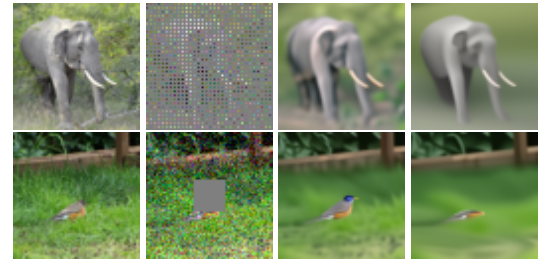


Figure 3. Noisy inpainting example. From left to right: original image, masked image, MAP-GA-PGDM(Algorithm 3,  $\sigma_y = 0.1$ ), PGDM( $\sigma_y = 0.1$ ). From top to bottom: *sr2x mask*, *box25 mask*

optimization process for the MAP objective in tasks that involve conditional generation. We show that the gradient of the MAP objective is tractable, allowing the use of gradient-based optimization methods. To use our framework in practice, we propose an algorithm with a multi-step gradient ascent strategy for MAP optimization. Since we use gradient-ascent (a simple first-order gradient-based method), we observed that it requires extensive tuning of the learning rate and other hyperparameters due to the challenging optimization objective. To address this, we propose practically effective algorithms, for image inpainting using our framework (which can be extended to other inverse problems). We validate our framework with extensive experiments on image inpainting across diverse mask settings.

## Acknowledgements

This work is part of the Marie Skłodowska-Curie Actions project *MODELAIR*, funded by the European Commission under the Horizon Europe program through grant agreement no. 101072559. The computations and the data handling were enabled by resources provided by the Na-

tional Academic Infrastructure for Supercomputing in Sweden (NAISS), partially funded by the Swedish Research Council through grant agreement no. 2022-06725. Bharath thanks Sebastian Gerard and Heng Fang for their feedback on improving the presentation of this paper.

## References

[1] Simon Arridge, Peter Maass, Ozan Öktem, and Carola-Bibiane Schönlieb. Solving inverse problems using data-driven models. *Acta Numerica*, 28:1–174, 2019. 1

[2] Ashish Bora, Ajil Jalal, Eric Price, and Alexandros G Dimakis. Compressed sensing using generative models. In *International conference on machine learning*, pages 537–546. PMLR, 2017. 1

[3] Benjamin Boys, Mark Girolami, Jakiw Pidstrigach, Sebastian Reich, Alan Mosca, and O Deniz Akyildiz. Tweedie moment projected diffusions for inverse problems. *arXiv preprint arXiv:2310.06721*, 2023. 3

[4] Hamadi Chihoui, Abdelhak Lemkhenter, and Paolo Favaro. Zero-shot image restoration via diffusion inversion, 2024. 3, 5, 7

[5] Hyungjin Chung, Jeongsol Kim, Michael Thompson McCann, Marc Louis Klasky, and Jong Chul Ye. Diffusion posterior sampling for general noisy inverse problems. In *International Conference on Learning Representations*, 2023. 1, 3

[6] Hyungjin Chung, Suhyeon Lee, and Jong Chul Ye. Decomposed diffusion sampler for accelerating large-scale inverse problems. *arXiv preprint arXiv:2303.05754*, 2023. 3

[7] Hyungjin Chung, Byeongsu Sim, Dohoон Ryu, and Jong Chul Ye. Improving diffusion models for inverse problems using manifold constraints. *Advances in Neural Information Processing Systems*, 35:25683–25696, 2022. 3

[8] Ian Goodfellow, Jean Pouget-Abadie, Mehdi Mirza, Bing Xu, David Warde-Farley, Sherjil Ozair, Aaron Courville, and Yoshua Bengio. Generative adversarial nets. *Advances in neural information processing systems*, 27, 2014. 1

[9] Jonathan Ho, Ajay Jain, and Pieter Abbeel. Denoising diffusion probabilistic models. *Advances in neural information processing systems*, 33:6840–6851, 2020. 1, 2

[10] Tero Karras, Miika Aittala, Timo Aila, and Samuli Laine. Elucidating the design space of diffusion-based generative models. *Advances in neural information processing systems*, 35:26565–26577, 2022. 2, 4, 5, 6, 7

[11] Bahjat Kawar, Michael Elad, Stefano Ermon, and Jiaming Song. Denoising diffusion restoration models. *Advances in Neural Information Processing Systems*, 35:23593–23606, 2022. 1, 3

[12] Andreas Lugmayr, Martin Danelljan, Andres Romero, Fisher Yu, Radu Timofte, and Luc Van Gool. Repaint: Inpainting using denoising diffusion probabilistic models. In *Proceedings of the IEEE/CVF conference on computer vision and pattern recognition*, pages 11461–11471, 2022. 6

[13] Alex Nichol, Prafulla Dhariwal, Aditya Ramesh, Pranav Shyam, Pamela Mishkin, Bob McGrew, Ilya Sutskever, and Mark Chen. Glide: Towards photorealistic image generation and editing with text-guided diffusion models. *arXiv preprint arXiv:2112.10741*, 2021. 1

[14] Deepak Pathak, Philipp Krahenbuhl, Jeff Donahue, Trevor Darrell, and Alexei A Efros. Context encoders: Feature learning by inpainting. In *Proceedings of the IEEE conference on computer vision and pattern recognition*, pages 2536–2544, 2016. 4

[15] Xinyu Peng, Ziyang Zheng, Wenrui Dai, Nuoqian Xiao, Chenglin Li, Junni Zou, and Hongkai Xiong. Improving diffusion models for inverse problems using optimal posterior covariance. In *Forty-first International Conference on Machine Learning*, 2024. 3

[16] Danilo Rezende and Shakir Mohamed. Variational inference with normalizing flows. In *International conference on machine learning*, pages 1530–1538. PMLR, 2015. 1

[17] Olga Russakovsky, Jia Deng, Hao Su, Jonathan Krause, Sanjeev Satheesh, Sean Ma, Zhiheng Huang, Andrej Karpathy, Aditya Khosla, Michael Bernstein, et al. Imagenet large scale visual recognition challenge. *International journal of computer vision*, 115:211–252, 2015. 6

[18] Chitwan Saharia, William Chan, Huiwen Chang, Chris Lee, Jonathan Ho, Tim Salimans, David Fleet, and Mohammad Norouzi. Palette: Image-to-image diffusion models. In *ACM SIGGRAPH 2022 conference proceedings*, pages 1–10, 2022. 1

[19] Jascha Sohl-Dickstein, Eric Weiss, Niru Maheswaranathan, and Surya Ganguli. Deep unsupervised learning using nonequilibrium thermodynamics. In *International conference on machine learning*, pages 2256–2265. PMLR, 2015. 1, 2

[20] Jiaming Song, Arash Vahdat, Morteza Mardani, and Jan Kautz. Pseudoinverse-guided diffusion models for inverse problems. In *International Conference on Learning Representations*, 2023. 1, 3, 5, 7, 8

[21] Yang Song and Prafulla Dhariwal. Improved techniques for training consistency models. *arXiv preprint arXiv:2310.14189*, 2023. 3

[22] Yang Song, Prafulla Dhariwal, Mark Chen, and Ilya Sutskever. Consistency models. *arXiv preprint arXiv:2303.01469*, 2023. 3, 4, 5, 6

[23] Yang Song and Stefano Ermon. Generative modeling by estimating gradients of the data distribution. *Advances in neural information processing systems*, 32, 2019. 3

[24] Yang Song, Sahaj Garg, Jiaxin Shi, and Stefano Ermon. Sliced score matching: A scalable approach to density and score estimation. In *Uncertainty in Artificial Intelligence*, pages 574–584. PMLR, 2020. 2

[25] Yang Song, Jascha Sohl-Dickstein, Diederik P Kingma, Abhishek Kumar, Stefano Ermon, and Ben Poole. Score-based generative modeling through stochastic differential equations. *arXiv preprint arXiv:2011.13456*, 2020. 1, 2

[26] Pascal Vincent. A connection between score matching and denoising autoencoders. *Neural computation*, 23(7):1661–1674, 2011. 2

[27] Ricardo Vinuesa and Steven L Brunton. Enhancing computational fluid dynamics with machine learning. *Nature Computational Science*, 2(6):358–366, 2022. 1

- [28] Hengkang Wang, Xu Zhang, Taihui Li, Yuxiang Wan, Tiancong Chen, and Ju Sun. Dmplug: A plug-in method for solving inverse problems with diffusion models. *arXiv preprint arXiv:2405.16749*, 2024. [1](#), [3](#), [5](#), [7](#)
- [29] Yinhuai Wang, Jiwen Yu, and Jian Zhang. Zero-shot image restoration using denoising diffusion null-space model. *arXiv preprint arXiv:2212.00490*, 2022. [3](#)
- [30] Raymond A Yeh, Chen Chen, Teck Yian Lim, Alexander G Schwing, Mark Hasegawa-Johnson, and Minh N Do. Semantic image inpainting with deep generative models. In *Proceedings of the IEEE conference on computer vision and pattern recognition*, pages 5485–5493, 2017. [4](#)
- [31] Yuanzhi Zhu, Kai Zhang, Jingyun Liang, Jiezhang Cao, Bihan Wen, Radu Timofte, and Luc Van Gool. Denoising diffusion models for plug-and-play image restoration. In *Proceedings of the IEEE/CVF Conference on Computer Vision and Pattern Recognition*, pages 1219–1229, 2023. [3](#)